Association Aéronautique et Astronautique de France

57th 3AF International Conference on Applied Aerodynamics
29 – 31 March 2023, Bordeaux - France

AERO2023-56-HANMAN

Aerodynamics of a CRM Joined-Wing Configuration at Transonic Speeds

Paul Hanman, Yufeng Yao and Abdessalem Bouferrouk

School of Engineering, University of the West of England, Bristol, BS16 1QY, United Kingdom
Emails: Paul.Hanman@uwe.ac.uk; Yufeng.Yao@uwe.ac.uk; Abdessalem.Bouferrouk@uwe.ac.uk

ABSTRACT

The presented work aims to showcase a joined-wing (JW) concept with key design parameters based on the NASA Common Research Model (CRM) configuration, to highlight its potential application for an efficient commercial transport or cargo aircraft flying at transonic speeds. The methodology of converting an existing CRM wing into a JW design is presented. The initial concept design is preceded by a parametric study to determine viable designs with aerodynamic design performed using panel code method VLMD (Vortex Lattice Minimum Drag). These designs are further analysed using CFD (Computational Fluid Dynamics) methods to inspect and show how the flow structures interact within the current JW design and if any unexpected beneficial or adverse effects are experienced. Since the cruise condition for the JW design lies in transonic flow conditions, analysis of shock structure and flow interaction around the joint location is analysed for any localised effects, along with other aerodynamic performances. It is found that a shock appears on the inboard side of the vertical fin, due to high incoming flow speed. This vertical fin also affects a delayed formation of shock on the outboard of main wing near the joint, and this effect reduces gradually towards the main wing tip region.

NOMENCLATURE

C_L – Coefficient of Lift
C_D – Coefficient of Drag
C_{Di} – Coefficient of Induced Drag
C_{DV} – Vortex Drag Coefficient
C_P – Coefficient of Pressure
D_i – Induced Drag
e – Wing Span Efficiency Factor
L_{scale} – Length Scale
M – Mach Number
S – Reference Wing Area
U_{bc} - Arithmetic average velocity at domain boundary
U_{domain} - Arithmetic average velocity over domain cells
V - Airspeed
α – Angle of Attack (AoA)
ρ – Density
η – Dimensionless Spanwise Length
Δt_u – Dynamic time-step
π – Constant
AR – Aspect Ratio
CFD – Computational Fluid Dynamics
CRM – Common Research Model
JW – Joined Wing
SST – Shear Stress Transport
UAV – Unmanned Aerial Vehicle
VLMD - Vortex Lattice Minimum Drag

1. INTRODUCTION

With the rise in requirements to reduce fuel consumption and emissions, aircraft manufacturers have been continually pushing the boundaries of the conventional cantilever aircraft design. Key questions to ask include: Have we reached the limits of current designs in terms of aerodynamic and engine efficiency? Are we reaching the point of diminishing returns by extending research current on configuration? And would unconventional configurations provide better returns on research and investment? One unconventional configuration that has emerged is the joined wing (JW) concept. Like the Strut-Braced Wing [1]–[3], the JW configuration increases the aspect ratio (AR) of the main wing, with structural support in the form of a, forward swept, extended rear wing joined with the main wing. This extended rear wing would also serve to replace the tail plane and as such will be used for pitching control purposes. Munk [4] highlighted that the JW design could be beneficial for both weight and induced drag reductions. Since the configuration involves introducing the rear wing as a structural supporting element, this allows the extension of the main wing in the spanwise direction, producing a longer main wing. This higher AR would reduce the induced drag for the same lift coefficient as seen from Eq. 1:

$$C_{D_i} = \frac{D_i}{\frac{1}{2}\rho V^2 S} = \frac{C_L^2}{\pi A R e} \quad (1)$$

Furthermore, other concepts such as the box wing and Prandtl wing configurations have also been tipped to produce 20-30% drag reduction depending on design. Additionally, Munk stated that the induced drag is

independent of leading-edge sweep angles implying that the JW configuration can be applied to all forms of aircraft design, commercial, military or general aviation. Some low-fidelity CFD simulations of joined wing and box wing aerodynamic analysis have been performed in the past at lower Mach numbers [1], [5]–[11], however these studies are for the purposes of developing joined/box wing UAV concepts and not for commercial applications. One such study [9] was performed at Mach 0.6 using low-fidelity CFD methods for a JW UAV rather than a commercial airplane. While an oblique shockwave was noted on the rear wing, further transonic effects such as leading-edge shock and compressible flow effects would be unlikely to occur at these conditions. This is also an effect that may be further pronounced at higher Mach numbers. Another paper [11] investigated structural analysis of the box wing at transonic conditions, although this analysis only focuses on the structural aspects of the box wing design.

Therefore, there is a gap of knowledge surrounding the JW design properties at higher Mach numbers, particularly under transonic conditions when shockwave appears and interacts with adjacent wings using high-fidelity CFD methods.

2. PURPOSE OF THIS STUDY

The purpose of this study is to investigate the shock characteristics at transonic speeds on the main and rear wings as well as around the joint location between the main and the rear wing of a newly developed JW design. This will be performed using CFD methods and comparing the flow and shock structures to the known platform of the NASA CRM (Common Research Model) [12]. Furthermore, the drag reduction due to the JW design will be investigated to realise whether the higher AR of both JW planform affects drag. Both the main and rear wings of the JW design will be investigated independently and jointly to determine individual wing performance, as well as the combined performance. These investigations will be carried out at a Reynolds number of 5 million at Mach 0.85, following the NASA CRM wind tunnel tests performed at the NASA's NTF (National Transonic Facility) [13].

3. METHODOLOGY

For this study, CFD solver ANSYS Fluent is used to assess the shock characteristics of each of the geometries at transonic conditions. The primary investigative geometries have been designed using a rudimentary adaption of the CRM planform, followed by an initial parametric study focused on minimum C_{Dv}, both of which are discussed. For the purposes of this discussion C_{Dv} is the same as C_{Di}.

3.1. JW Design

The initial JW design methodology involved a simple adaption of the CRM planform to fit a JW shape. For the sake of aerodynamic similarity in this initial phase, the total planform area of the CRM was kept as a constant value to be transferred over to the JW design. This included the tail planform area, bringing the initial JW area to 464.515m^2. Keeping the total area as a constant during a parametric design study that varied key parameters of the main wing and the joint location. The design C_L of 0.5 at Mach 0.85 was also retained for the JW design. The key parameters varied are shown in Tab. 1. Once the initial variables were studied, further iterations of the parametric study were performed to produce a final planform geometry.

Table 1: Parametric Study Variables.

Variable	*Range*
Span (m)	29.38-40
Root Chord (m)	6-9
Join Location (η)	0.4-0.9
Tail Height (Above Main Wing root) (m)	2.027-13.739

The VLMD [14] code, used for initial JW wing design, takes a wing planform and design C_L as an input, and outputs twist and camber distribution to meet the pre-defined design C_L, along with a predicted drag coefficient C_{Dv} value, equivalent to lift-induced drag coefficient. The parametric study developed multiple planforms over the variable ranges, with the purpose to identify a planform that produces the lowest value of C_{Dv} for a given design C_L of 0.5 at Mach 0.85 (i.e. CRM design point).

3.2. Geometries

Three main geometries are used in the present study: the CRM wing body configuration, the JW main wing only, and the JW with both wings and a vertical fin as a connecting joint. The final JW geometry used for this study can be seen in Fig. 1, with a close-up of the joint location in Fig. 2 and primary dimensions of both the main and rear wings in Tab 2.

Table 2: JW63a Geometry Parameters.

JW63a	*Main Wing*	*Rear wing*
Span (m)	40	28
Root Chord (m)	7	3.94
Dihedral (Degrees)	7	4.921
Taper Ratio	0.2	0.6
Joint Location (% Span)	0.7	
AR	22.21	17.78
Sweep Angle (Degrees)	35	-18

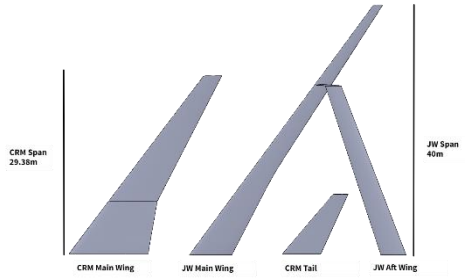

Figure 1: CRM and JW geometries (not in scale).

The main and rear wings of the JW63a geometry were generated from mapping the VLMD design outcomes (twist and camber) onto the CRM thickness distributions for an initial design. From VLMD this design configuration produces a predicted C_{Dv} of 0.001895 for a design C_L of 0.5.

The joint between the two wings shown in Fig. 2 is composed of a symmetric aerofoil developed as a vertical fin. The purpose of this vertical fin is to investigate the aerodynamic effects of the fin on the main and rear wings and the shock characteristics associated with the fin. The overall joint has not yet been optimised and as such is a simple symmetric aerofoil stack (NACA 0008) lofted onto the tip of the rear wing to create a joint. The vertical fin is 1 meter in height and begins at 0.11 *x/c* (here *x* and *c* are local streamwise coordinate and chord length respectively) from the leading-edge of the main wing section. The fin is also in alignment with the incoming flow direction.

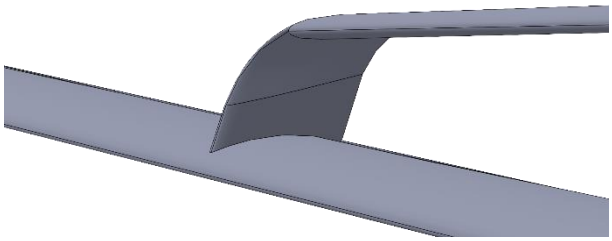

Figure 2: Initial Joint modelled as a vertical fin.

The rear wing also uses the same thickness distribution as the CRM tail wing, which is noted to be a symmetrical aerofoil with root thickness of 10% to a tip thickness of 8%.

3.3. CFD Settings and Flow Conditions

All simulations utilised the *k-ω* SST (Shear Stress Transport) turbulence model as this has a good application for transonic flow and shock characteristics [15]. Due to the complexity introduced by the joint in the 3D flow simulations, and considering the limited past available research, the simulations were setup using pseudo-transient settings to assist in resolving any small transient flow issues that may be present during the solution at transonic flow conditions. An initial length scale was set according to the MAC (Mean Aerodynamic Chord) of the main wing with a time scale factor of 5, used to set a global time-step. If instability in either of the monitored values of lift or drag was still present after the initial phase of iterations, then the length scale was reduced to a length equal to the tip of the main wing and the time scale factor adjusted in accordance with Eq. 2. Where Δt_u is the dynamic time-step, the velocity U_{bc} is the maximum of the arithmetic average of the velocity at the domain boundary faces, and U_{domain} is the arithmetic average of the velocity over the cells in the domain [16].

$$\Delta t_u = \frac{0.3 L_{scale}}{MAX(U_{bc}, U_{domain})} \quad (2)$$

All geometries were simulated with a chord Reynolds number of 5 million at M = 0.85 and at angles of attack (AoA) of 2.5, 3.25, 3.5, 3.75 and 4 degrees respectively, to provide lift and drag results, in accordance with the NTF test conditions for the CRM experiment. This is with exception to the CRM wing body geometry, which will only be run at 2.5 degrees to provide validation data for C_P results. Full validation using the wing body geometry has been performed against the NTF data, however, will not be presented in this paper. The primary results of the main wing, and JW configurations, including the flow analysis of the join location will be performed at 2.5 degrees AoA only.

3.4. Flow Domain and Mesh Generation

The flow domain used for the mesh is shown in Fig. 3. A semi-spherical domain was chosen for the ease of altering the flow angle with a far-field inlet boundary. The far-field boundary was set-up with a flow Mach number of 0.85, with an operating pressure of 5072.49 Pascal and an inlet temperature of 322.04 Kelvin. Turbulence settings were kept as default and incoming flow angle altered using Cartesian coordinates as required.

Mesh generation was completed using the Fluent meshing software. Each geometry had a mesh generated with similar nodal distribution and mesh resolution. This resulted in a mesh of approximately 14 million elements for the JW geometry. Mesh generation used a hybrid Poly-Hexacore mesher which produces polyhedral elements at domain interfaces and hexacore elements in the remaining larger volume regions such as the free stream of the domain. This hybrid structured-unstructured mesh allows for quicker mesh generation than a fully structured mesh, while also producing faster computational times without sacrificing on solution accuracy. This mesh generation type was also chosen to

alleviate edge-sizing issues discovered in the earlier stages of mesh generation that used tetrahedral meshing.

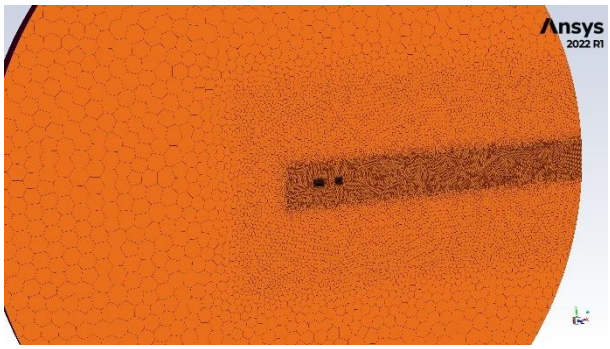

Figure 3: Computational domain (a semi-sphere with radius of 400m) and mesh of JW63a design.

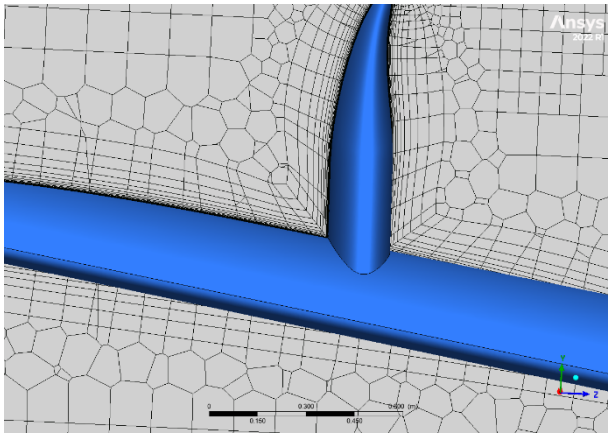

Figure 4: Volume, boundary layer and surface meshes around the main wing and joint location.

Mesh size was refined towards and around both wings and the joint location incrementally as it approaches the geometry. Fig. 3 also shows the overall polyhedral elements in the domain, while Fig. 4 shows the poly-hexacore transition and how the hexacore mesh is resolved from the surface mesh to the volume mesh. The initial boundary layer height was determined from the test conditions and a $y^+ \sim 1$ on wing surfaces. This results in the first layer thickness height of 3×10^{-5}m.

3.5. CFD Validation

These results were modelled with the fuselage present for validation purposes, with lift coefficient shown in Fig. 5 which shows good agreement for all angles of attack (-3 to 7 degrees). Fig. 6 shows the pressure coefficient distributions along the span of the main wing for the baseline CRM geometry at 2.5 degrees. These are plotted against the experimental data at the same conditions, specifically run 44 (R44) of the NTF wind tunnel experiments [13]. They show good correlation to the experimental results and follow the same discrepancies as seen by other CFD validation studies performed on CRM [17], specifically in the higher suction seen towards the tip in the simulated results, although the authors did not provided any explanation for these discrepancies.

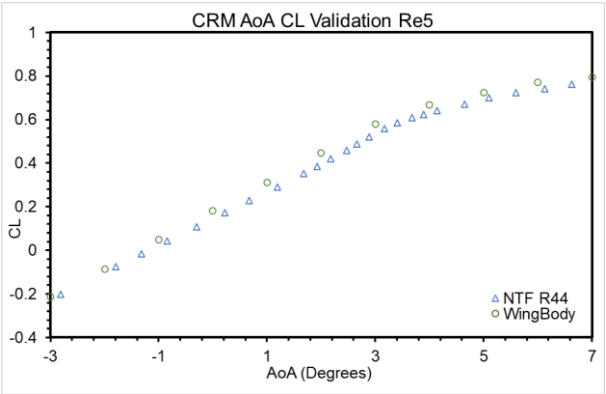

Figure 5: CRM C_L validation results.

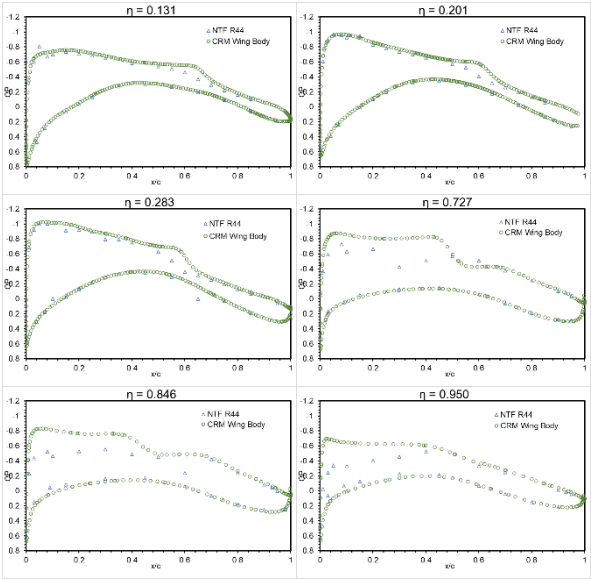

Figure 6: Pressure coefficient distributions at different spanwise locations, $\alpha = 2.5^{o}$

Furthermore, the pressure coefficient contours shown in Fig. 7 exhibit reasonable correlation with the computed pressure contours by Vassberg et al. [12] generated in OVERFLOW and presented in Fig. 8. It should be noted that the experimental pressure isobars have an inverse colour gradient for the contour legend. Further validation has been performed at multiple angles of attack to ensure validity of these methods as shown in Fig. 5. Therefore, it can be concluded that the CFD method used are appropriate for this study.

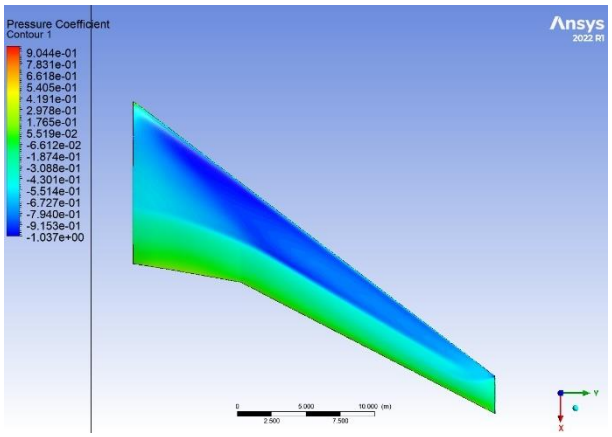

Figure 7: CRM wing body numerical C_P contours at α = 2.5 °.

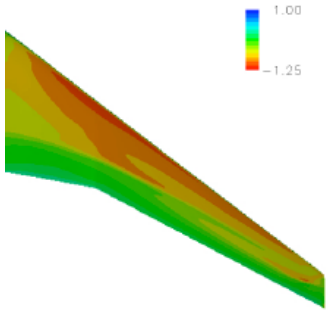

Figure 8: CRM C_P contours at α = 2.5 ° from Vassberg et al. [12].

4. RESULTS AND ANALYSIS

Once validation is established, the next results obtained from CFD will mostly focus on lift and drag, pressure coefficient plots, contour diagrams and analysis of the flow structures in the vicinity of the joint. The shock structure around the joint will also be analysed to show any major features.

4.1. Lift, Drag and Pressure Analysis

The main wing of the JW is investigated for aerodynamic characteristics at transonic conditions. This is also done to investigate the characteristics of the wing without the joint in order to compare how the joint may affect the main wing in a later comparison. Figs. 9-10 shows the lift and drag coefficient data against AoA for all the configurations tested.

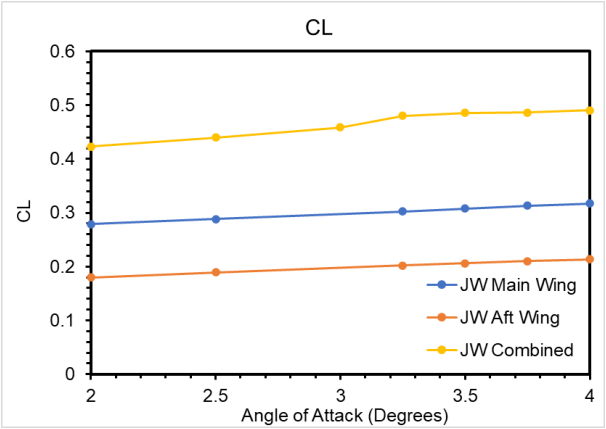

Figure 9: C_L variations with AoA for different wing configurations.

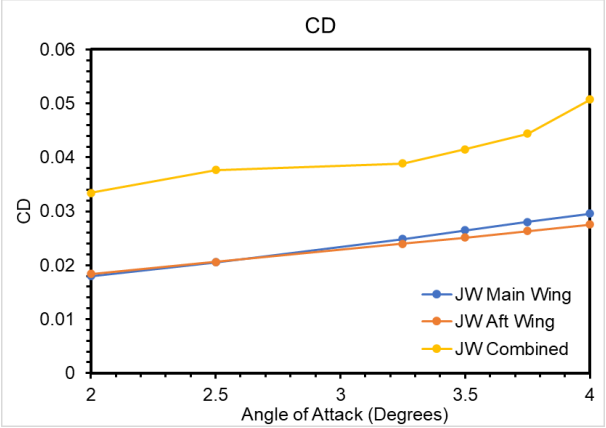

Figure 10: C_D variations with AoA for different wing configurations.

From the C_L values in Fig. 9, we can calculate the induced drag of the main wing using Eq. 1. The values of C_L and *AR* are known, while e can be estimated to 0.8 [18]. The calculated C_{Di} for each angle is shown in Tab. 3.

Table 3: JW Main wing C_{Di} calculations.

Angle (degree)	C_L	C_{Di}
2.5	0.288	0.00139
3.25	0.302	0.00149
3.5	0.308	0.00164
3.75	0.313	0.00170
4	0.318	0.00175

Fig. 11 shows the C_P graphs that compare between the JW main wing and in the full JW configuration i.e. including the vertical fin at a location η = 0.7 for the joint configuration. The C_P graphs are indicative of the aerofoil design with a noticeable shock location along the span, which is better visualised in Fig. 13.

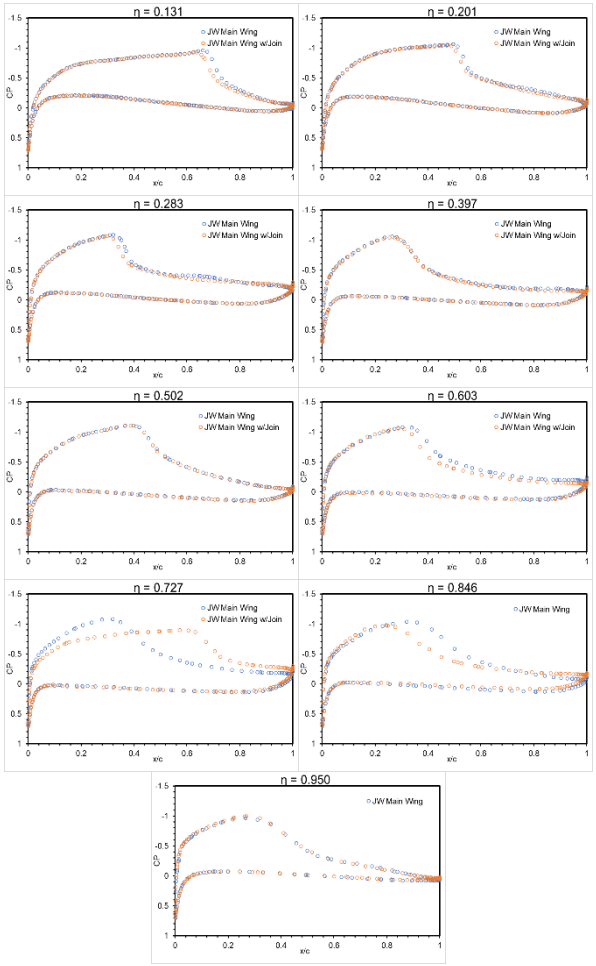

Figure 11: C_p comparison the JW main wing in presence of the joint.

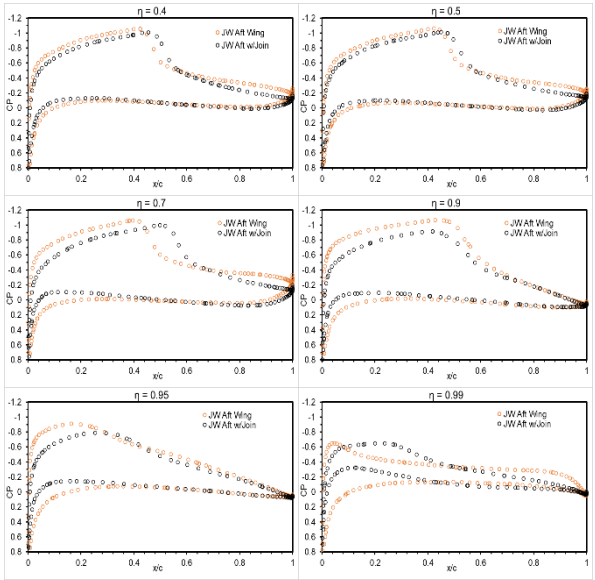

Figure 12: C_p comparison of the JW rear wing in presence of the joint.

The C_p values remain the same or very similar up to the joint location ($\eta = 0.7$), with a restructuring of the flow beyond the joint. The C_p plot at $\eta = 0.727$ shows the greatest difference due to the effect of the joint, with a delay to the shock similar to that produced by a supercritical aerofoil, or that of a fuselage-wing junction. Figs. 13-14 shows this comparison between the two configurations as surface contours on the main wing and the JW configuration respectively. This shows, along with the C_p plots, that the C_p values remain consistent up until the junction between the main and rear wings. For the rear wing, Fig. 12 shows there is a general delay in the shock when introduced with the main wing, however, the greatest difference is seen towards the tip of the rear wing whereby the C_p is clearly affected by the presence of the vertical fin, seemingly decreasing and delaying the point of maximum suction at the tip. This may result in increasing the strength of the vortex developed by the tip of the rear wing. Fig. 15 shows a close-up view of the C_p contours at the wing junction on the upper surface of the main wing.

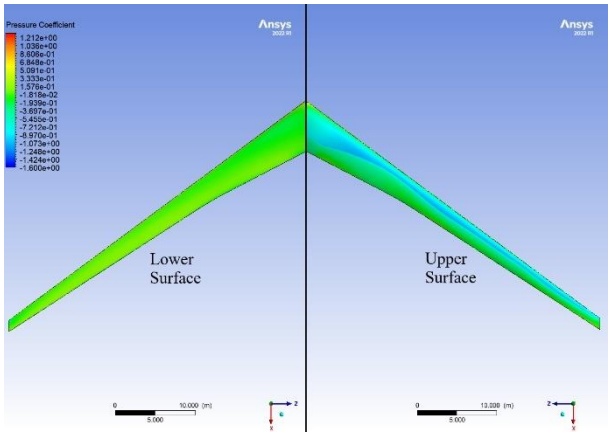

Figure 13: C_p contours on upper and lower surfaces of JW main wing.

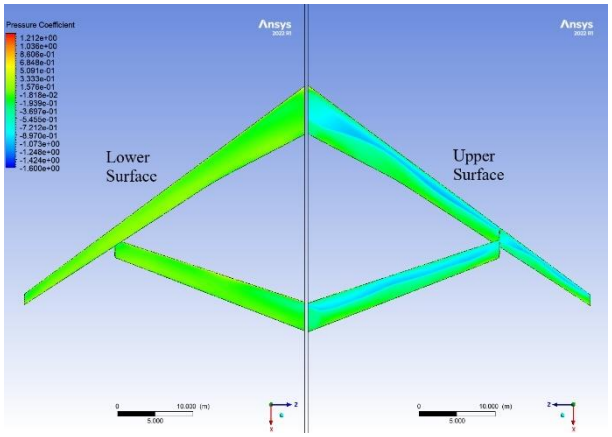

Figure 14: C_p contours on upper and lower surfaces of JW design.

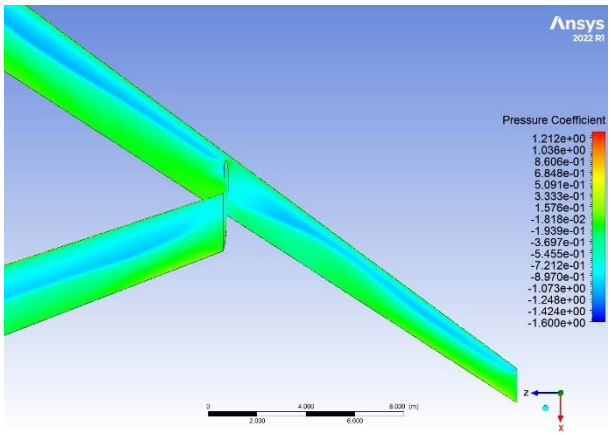

Figure 15: C_p contours on upper surfaces of JW design at the tip.

From Fig. 15, and the C_p plot comparison at $\eta = 0.727$ in Fig. 11, we can see that the flow has greater attachment beyond the point of the junction, as well as a reduction in the aerodynamic shock experienced at that point along the span as evidenced by the delay in the increase in C_p along the chord. Furthermore, Fig. 16 shows an inboard shock propagating from the leading edge of the vertical fin. Note that this shock is only present on the inboard side of the vertical fin leading to speculation that this is due to outwash from the wing sweep creating a compression point on the inboard side of the leading edge of the vertical fin, resulting in a shockwave on the vertical fin. While under straight and level flight this may not have any adverse effect, however, there may be adverse yaw effects at these conditions due to this inboard shock. It should also be noted that the shock formed on the junction is stronger than the shock seen on the main or rear wings.

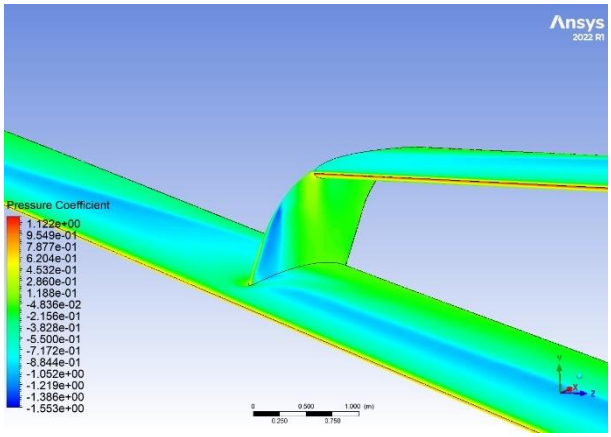

Figure 16: C_p contours on the vertical fin.

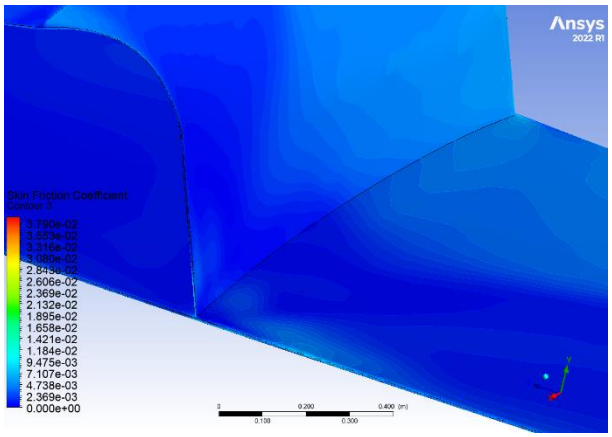

Figure 17: Skin friction coefficient contours on upper surfaces of JW and around the rear of the joint.

Figure 17 shows skin friction contours on the outboard side of the joint, showing similar patterns exhibited by CRM at the wing-fuselage junction [19]. This is also evident from Figs. 15-16 showing the C_P contours on the outboard side of the wing junction in similarity to the C_P contours towards the root of the main wing. This may imply that a vertical fin design is beneficial for the lift generated by the main wing due to this reattachment of airflow caused by the junction. Furthermore, the area of flow circulation was observed at the trailing edge of the vertical fin as seen from the inserted sub-figure in Fig. 18. Note that the streamline starting in the region of flow circulation exits the flow circulation and travels spanwise along the trailing edge of the main wing in an area of flow separation caused by the shock on the main wing.

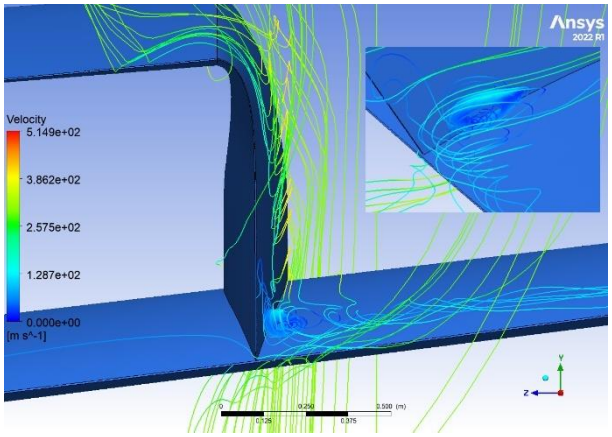

Figure 18: Velocity streamlines around the vertical fin trailing edge with zoomed in view (rear view).

The preliminary transonic work on a PrandtlPlane transport aircraft [6] highlighted a similar effect at the wing-fuselage junction. This effect was reduced by adding a fillet around the junction, which may also be beneficial for this isolated join design. Additionally, the flow interference with the vertical tip joint of the

PrandtlPlane shows similarity to the effects seen on the inboard side of the vertical fin of JW63a seen in Fig. 16.

Further analysis was performed on the vertical fin. This analysis investigates the flow structures around the vertical fin, and compares this analysis to the main wing. As such, Fig. 18, combined with the inserted sub-figure, shows velocity streamlines around the vertical fin, main wing and rear wing tip. These figures highlight the flow interaction with the vertical fin.

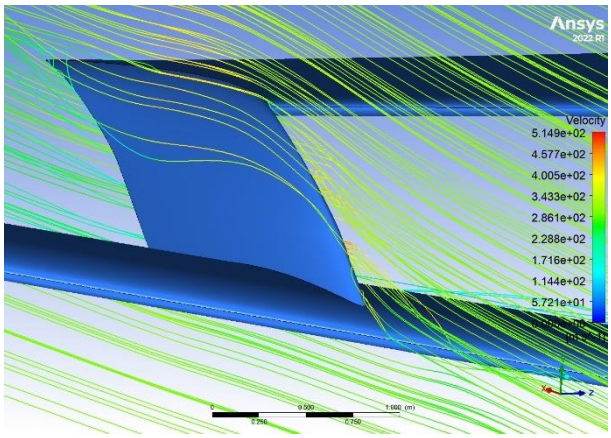

Figure 19: Velocity streamlines around the vertical fin (front/side view).

The streamlines shown in Fig. 19 show that the flow approaching the vertical fin has preference to flow towards the inboard side of the fin, likely due to the low-pressure region on the inboard side of the fin that has been previously discussed. This may increase the vortex generated by the rear wing by the shift in flow direction caused by the shockwave on the vertical fin. Also, note at the rear wing tip trailing edge a vortex can be clearly seen to begin from this location. This may be mitigated by improving the vertical fin design by creating a cleaner junction between the rear wing tip and the vertical fin.

Fig. 20 shows a vortex core region applied over the domain and highlights the areas of flow separation due to shockwave of the individual main wing. The vortex core region has Mach number overlaid on top to highlight the region of high-speed flow over the main wing. As can be seen, the greatest section of flow separation, other than at the wing tip, occurs between $\eta = 0.3$ and $\eta = 0.4$ where the shock detached closest to the leading edge. This is likely due to lack of optimisation on the main wing and could be improved, thereby potentially increasing the lift generated by the wing while also reducing the drag from the shock induced separation.

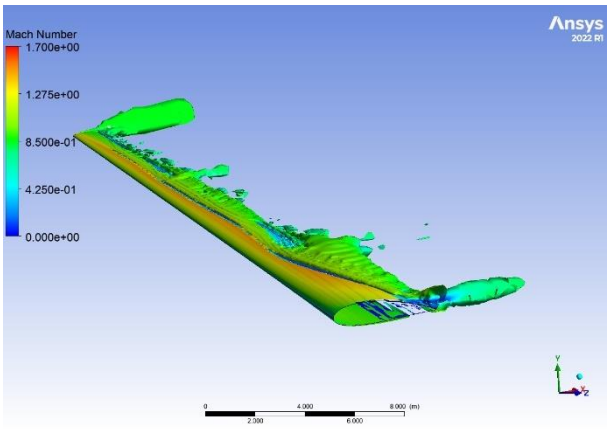

Figure 20: Vortex core region with Mach number colouring of JW main wing.

Comparing to a vortex core region overlaid on the JW configuration as shown in Fig. 21, the JW configuration also produces a large vortex at the joint location, like that produced towards the root of the main wing. As previously discussed, further optimisation of the main wing would reduce this inboard vortex and potentially isolate the larger instances of generated vortices to the main wing tip and vertical fin junction. It can also be noted that the main wing tip vortex is unaffected by the presence of the join. This is also reflected in the reduction of differences in C_p between the two configurations at the wing tip.

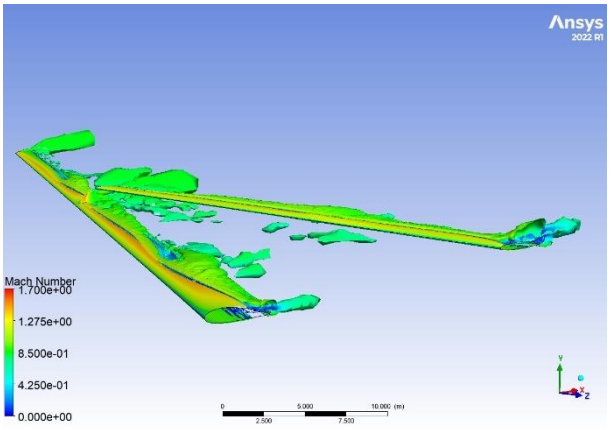

Figure 21: Vortex core region with Mach number colouring of JW design.

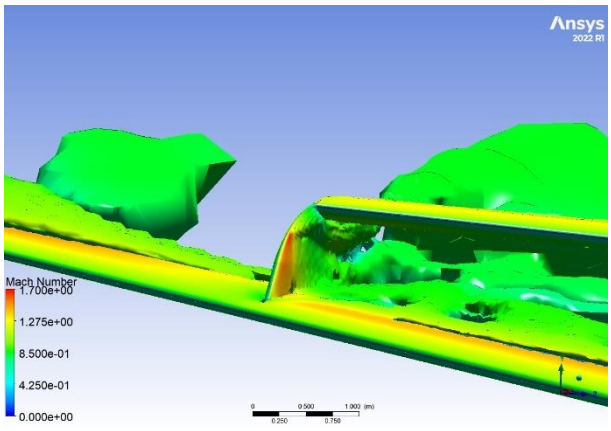

Figure 22: Vortex core region with Mach number colouring of JW joint close-up view.

Further examination of the vortex core regions (Fig. 22) shows the trailing edge flow interaction between the vertical fin and the main wing is a significant cause of wake vortices. This may be influenced by the sharp junction at the trailing edges and may benefit from a filleted junction, or from careful redesigning of the vertical fin as this may be a cause of the shock seen on the vertical fin as previously discussed. The shock would be the cause of increased flow separation and therefore increased pressure drag. A different design of this join may mitigate this effect or even nullify any drag penalty incurred by the vertical fin due to the leading-edge shock. As previously discussed, the stronger shock produced by the junction can be seen in the Mach number contours overlaid on top of the vortex core region. This means there is a significant acceleration of flow over the leading edge of the vertical fin, potentially due to the flow conditions, the incidence of the shockwave on the main wing and the transversal flow from the main wing. This design implementation therefore may require further investigation to determine the nature of this flow acceleration and if there are any mitigating factors that can be implemented for this specific design.

5. CONCLUSION

This study presents a numerical methodology for a joined wing design and analysis. The JW wing has a vertical fin joint between the main and rear wing. The JW configuration was obtained following a parametric study using low-fidelity panel codes, guided by known aerodynamic performance of the CRM geometry at transonic speeds. The obtained JW geometry was then analysed using pseudo transient CFD simulations, first to validate the numerical approach and second to investigate the flow and shock characteristics at Mach 0.85, focusing mainly on the effects of the joint. In doing so, the JW design was compared to the main wing only geometry to clearly isolate the impact of the vertical fin. The rear wing was also analysed and was shown to have an effect along the span due to the presence of the main wing, and a significant reduction in C_P towards the tip where the vertical fin joint begins.

The C_P of the main wing was found to have both reduced the shock and increased the delay in the shock in the section of wing immediately outboard of the vertical fin. This delay of the shock showed greater flow attachment at that location when compared to the main wing only, potentially having a positive effect on the local lift and drag. This effect dissipated towards the main wing tip, with the C_P plot closest to the tip showing no difference between the geometries.

An area of flow separation was observed on the outboard trailing edge of the vertical fin. As discussed, this shows similar correlation to fuselage-wing junctions and as such similar design considerations could be considered to reduce this effect.

A strong shock was observed on the inboard side of the vertical fin whereby an increase in flow separation was seen, and where the incoming flow was favouring the inboard side, potentially increasing the generated vortex. This shock is also likely to have been produced by the flow conditions and transversal flow from the main wing. Furthermore, this shock was stronger than the shock seen on the main wing.

6. FUTURE RECOMMENDATIONS

This study has highlighted certain aspects of analysis that could benefit from future work. Notably, the further investigations of the flow characteristics surrounding the join location and the implications of shockwave effects on the join. Furthermore, different join designs could have differing effects on flow characteristics, some of which may be beneficial to future designs and may reduce the effect of some of the characteristics observed in this study.

Future work is currently underway regarding different JW configurations. While the JW configuration used for this study was the best in terms of C_{DV} produced by VLMD, further designs are being developed and investigated to determine their suitability for real-world applications.

Further work is needed on optimising the main wing design. Since VLMD is a vortex lattice code, viscous and Mach/shock effects are not accounted for in the twist and camber design produced by VLMD and is therefore not the most suitable for finalising the design.

The irregular and variable shock locations along the span of the main wing also require closer examination or optimisation, perhaps using a different aerofoil designed for transonic conditions should also be investigated for optimisation purposes. Care needs to be taken on the

potential adverse yaw effect at transonic conditions due to the inboard shock observed on the vertical fin, which presumably would also have implications for aircraft stability. However, a different join design may mitigate this as a potential issue.

Acknowledgement: The authors would like to acknowledge the partial financial support from Engineering Modelling and Simulation Research Group (https://www.uwe.ac.uk/research/centres-and-groups/emsg) in making this paper possible.

7. REFERENCES

[1] R. Cavallaro and L. Demasi, "Challenges, Ideas, and Innovations of Joined-Wing Configurations: A Concept from the Past, an Opportunity for the Future," *Prog. Aerosp. Sci.*, vol. 87, pp. 1–93, 2016, doi: 10.1016/j.paerosci.2016.07.002.

[2] J. Xiong, J. Fugate, and N. Nguyen, "Investigation of Transonic Truss-Braced Wing Aircraft Transonic Wing-Strut Interference Effects using Fun3D," *AIAA Aviat. 2019 Forum*, pp. 1–19, 2019, doi: 10.2514/6.2019-3026.

[3] N. R. Secco and J. R. R. A. Martins, "RANS-based aerodynamic shape optimization of a strut-braced wing with overset meshes," *J. Aircr.*, vol. 56, no. 1, pp. 217–227, 2019, doi: 10.2514/1.C034934.

[4] M. Munk, "Minimum Induced Drag of Aerofoils," *NACA*, no. 121, 1923, [Online]. Available: https://ntrs.nasa.gov/citations/19800006779

[5] H. Djojodihardjo and K. E. Foong, "Conceptual Design and Aerodynamic Study of Joined-Wing Business Jet Aircraft," no. May, 2014, [Online]. Available: https://www.researchgate.net/publication/254862073_Conceptual_Design_and_Aerodynamic_Study_of_Joined-Wing_Business_Jet_Aircraft

[6] V. Cipolla, A. Frediani, K. Abu Salem, V. Binante, E. Rizzo, and M. Maganzi, "Preliminary transonic CFD analyses of a PrandtlPlane transport aircraft," *Transp. Res. Procedia*, vol. 29, pp. 82–91, 2018, doi: 10.1016/j.trpro.2018.02.008.

[7] D. S. Sahana and A. Aabid, "CFD Analysis of Box Wing Configuration," *Int. J. Sci. Res.*, vol. 5, no. 4, pp. 706–709, 2016, doi: 10.21275/v5i4.nov162673.

[8] S. C. Smith and R. K. Stonum, "Experimental aerodynamic characteristics of a joined-wing research aircraft configuration," *Nasa Tech. Memo.*, 1989, [Online]. Available: http://archive.org/details/nasa_techdoc_19890014914

[9] R. Sivaji, "Aerodynamic Analysis of the Joined-Wing Configuration of a High-Altitude, Long Endurance (HALE) Aircraft," University of Cincinnati, 2004. [Online]. Available: http://rave.ohiolink.edu/etdc/view?acc_num=ucin1083849791

[10] P. O. Jemitola and P. P. Okonkwo, "An Analysis of Aerodynamic Design Issues of Box Wing Aircraft," *Glob. J. Res. Eng. A Mech. Mech. Eng.*, vol. 22, no. 1, 2022.

[11] P. Jemitola and P. Okonkwo, "Review of Structural Issues in the Design of a Box Wing Aircraft," *J. Aerosp. Eng. Mech. Open Access*, vol. 3, no. 1, pp. 161–166, 2019.

[12] J. C. Vassberg *et al.*, "Development of a Common Research Model for Applied CFD Validation Studies," p. 6919, 2008, doi: 10.1109/ivelec.2006.1666254.

[13] M. B. Rivers and A. Dittberner, "Experimental investigations of the NASA common research model," *J. Aircr.*, vol. 51, no. 4, pp. 1183–1193, 2010, doi: 10.2514/1.C032626.

[14] E. Lamar, "A Vortex-Lattice for of the Mean Method Shapes Drag Trimmed Minimum Vortex With Minimum Vortex Drag," 8090, 1976. [Online]. Available: https://ntrs.nasa.gov/citations/19760019073

[15] Ansys Fluent, "Modeling Turbulent Flows," *Fluent user Guid.*, p. 49, 2006, [Online]. Available: http://www.southampton.ac.uk/~nwb/lectures/GoodPracticeCFD/Articles/Turbulence_Notes_Fluent-v6.3.06.pdf

[16] ANSYS FLUENT 13 User's Guide, "Ansys Fluent Theory Guide," *ANSYS Inc., USA*, vol. 15317, no. November, pp. 724–746, 2013.

[17] L. C. Scalabrin and R. F. de Souza, "Grid assessment using the NASA common research model (CRM) wind tunnel data," *51st AIAA Aerosp. Sci. Meet. Incl. New Horizons Forum Aerosp. Expo. 2013*, no. January, pp. 1–18, 2013, doi: 10.2514/6.2013-52.

[18] D. Raymer, *Aircraft Design: A Conceptual Approach*, 2nd ed. American Institute of Aeronautics and Astronautics, 1992. doi: 10.2514/4.105746.

[19] D. Hue, Q. Chanzy, and S. Landier, "DPW-6: Drag analyses and increments using different geometries of the common research model airliner," *J. Aircr.*, vol. 55, no. 4, pp. 1509–1521, 2018, doi: 10.2514/1.C034139.